Title: **Innovative Approach in the Development of Computer Assisted Algorithm for Spine Pedicle Screw Placement**

Giovanni F. Solitro[1], Farid Amirouche[1]

1) Department of Orthopaedics, University of Illinois at Chicago, Chicago, IL

Please address all correspondence to: Giovanni F. Solitro, PhD

Research Associate

Department of Orthopaedics

University of Illinois at Chicago

835 S. Wolcott Ave., Room E270

Chicago, IL 60612

Phone: (312) 413-4674

Fax: (312) 413-3967

Email: gsolitro@uic.edu

Word count: 3773

KEYWORDS: spine, screw fixation, screw malposition, computer assisted surgery

## Abstract

Pedicle screws are typically used for fusion, percutaneous fixation, and means of gripping a spinal segment. The screws act as a rigid and stable anchor points to bridge and connect with a rod as part of a construct. The foundation of the fusion is directly related to the placement of these screws. Malposition of pedicle screws causes intraoperative complications such as pedicle fractures and dural lesions and is a contributing factor to fusion failure. Computer assisted spine surgery (CASS) and patient-specific drill templates were developed to reduce this failure rate, but the trajectory of the screws remains a decision driven by anatomical landmarks often not easily defined. Current data shows the need of a robust and reliable technique that prevents screw misplacement. Furthermore, there is a need to enhance screw insertion guides to overcome the distortion of anatomical landmarks, which is viewed as a limiting factor by current techniques. The objective of this study is to develop a method and mathematical lemmas that are fundamental to the development of computer algorithms for pedicle screw placement. Using the proposed methodology, we show how we can generate automated optimal safe screw insertion trajectories based on the identification of a set of intrinsic parameters. The results, obtained from the validation of the proposed method on two full thoracic segments, are similar to previous morphological studies. The simplicity of the method, being pedicle arch based, is applicable to vertebrae where landmarks are either not well defined, altered or distorted.


## Highlights:

1. Pedicle screw malposition is seen as contributing factor to failure.
2. Anatomical landmarks dictate the trajectory of the screws.
3. Safe screw insertion trajectories are evaluated using automated procedure.
4. Intrinsic parameters and insertion cross-section areas for pedicle screw are identified and computed.
5. The optimal trajectory is computed and suggested for use with “Computer assisted spine surgery” and “free hand” insertions.

## 1 Introduction

In thoracic deformity correction surgery the use of pedicle screws is becoming largely adopted [1] despite the intraoperative complications such as pedicle fractures (13%), dural lesions (12.1 %) and the postoperative fusion failure (4.3%)[2]. Hicks et al. [3] performed a systematic review of 12248 pedicle screws and found that 4.3% were reported as malpositioned. In the short term malpositions are asymptomatic, and the actual percentage of such irregularity is often underestimated. In fact, this percentage is estimated to be higher than 15.7% if Computed Tomography (CT) is used to evaluate the screw placement. Using CT, Privitera et al. [4], performed another study examining 1042 screws and reported 8.3% to have been misplaced, with the upper thoracic levels T1 and T2 showing the highest malposition rates of 28.6% and 18.2% respectively. Cardoso, using CT scans, identified the structures at risk of screw malposition placement [5]. Complications were seen in the esophagus (greater at T2), trachea (greater at T3) and Bronchus (greater at T4). To limit the malposition rate, computer-assisted spine surgery (CASS) and patient-specific drill templates were developed. Verma et al. [6] reviewed 23 studies from 1997 to 2007 for a total of 5992 pedicle screws and found that pedicle screws implanted by CASS had greater accuracy than conventional placement technique. Furthermore, he found that the neurological complications using CASS were less but not statistically significant (p = 0.07). In another study, Lu et al. [7], using patient specific templates of 16 scoliosis patients, found that only 1.8% of the screws were misplaced, and most of the screws were safe. Despite the accuracy achieved with CASS or patient specific templates, the trajectory of the screws remains at the discretion of the surgeon. The planning is mostly performed on 2D CT-based images combined with basic manipulations and generic anatomical markers/indicators (Figure 1) [7,8].

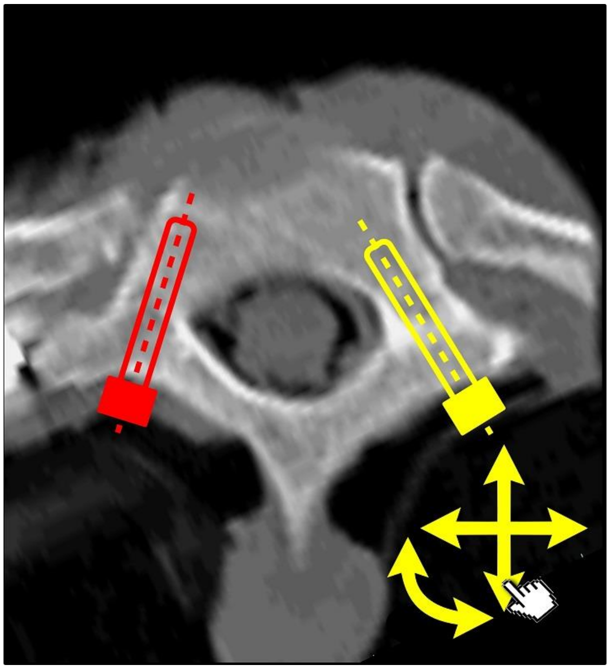

**Fig.1 2d Visualization of Screw placements on axial CT image of T1.**

In the past, anatomical studies have been performed focusing on the identification of the screw insertion site and the proper screw trajectories for better fixation and reduction in breaching.

Lehman et al.[9,10] differentiated between a straight-forward insertion in which the sagittal angulation of the screw is parallel to the superior endplate of the vertebral body, and an anatomic insertion trajectory, that follow the sagittal angle of the pedicle axis at a convergent angle of 22°.

The straight-forward technique was later used by Kim [11], where the insertion point is presumed to move more lateral and caudal from T12 to T1 with an average convergent transverse angle of 15.3°. Using the anatomical technique without image guidance, Elliot achieved full pedicle containment of the 5mm screws in only 87.5% of the specimens [12].

A more focused study on the screw placement angulation was performed by Zindrick et al. [13]. They reported transverse angle variation from a convergent value of 26.6°±5.6° at T1 to a divergent value of 4.2°±9.5° at T12, and a variation of sagittal angle from 12.6°±5.8° at T1 to 11.6°±2.6° at T12. Similarly, Lien et al. [14] using CT data and cadaveric dissections, reported an average pedicle transverse convergent angle of 28.6° at T1 that progressively decreases to 7.9°. Furthermore, he found that the pedicle safe zone dimension has a maximal width of 8.5±1.5 mm at T12 and a minimal width of 3.4±0.6 mm at T4. A first analytical approach has been adopted by Rampersaud et al. [15] to evaluate the required screw placement accuracy. Both pedicles and screws are modeled using cylinders with a dimension of 5 mm for the screws and average diameter value computed from 24 morphological studies. Rampersaud found that the allowable distance from the central axis of the pedicle varied from 1.5 mm at T1 to 0.5 mm at T12 with a virtual minimum of -0.05 mm at T5. The allowable angular deviation from the pedicle axis varied from 7.7° at T1 to 2.5° at T12.

The variability highlighted in these studies indicates the need of an algorithm that can be used and adopted on a case-by-case basis. Such algorithm is specifically needed, in cases where the distortion of anatomical landmarks limits the applicability of previous morphological studies [16].

This paper aim is to automate and significantly reduce the time of surgical planning, through the execution of sequential steps, for a given vertebra, identifying the screw trajectories and calculating the parameters, which yield the optimum screw insertion trajectory. The calculated trajectories are provided in an output format defined by the position of the entry point and its orientation, and can be used with CASS, patient specific templates and free hand approach.

## 2 Methods

### 2.1 Algorithm Framework

The overall framework of the methodology developed for pedicle screw insertion is shown in figure 2. It is divided into several steps where the blocks define the local computation and analysis required to proceed or interface with the others. The method makes use of data that is commonly available to clinicians/surgeons. The main computer-assisted tasks are identified in the following steps: reference frame and region of interest identification (ROI), cross sections discretization, trajectories calculation, safe trajectories filtering, numerical parameters calculation and selection. What follows is the description to each of the steps outlined above.

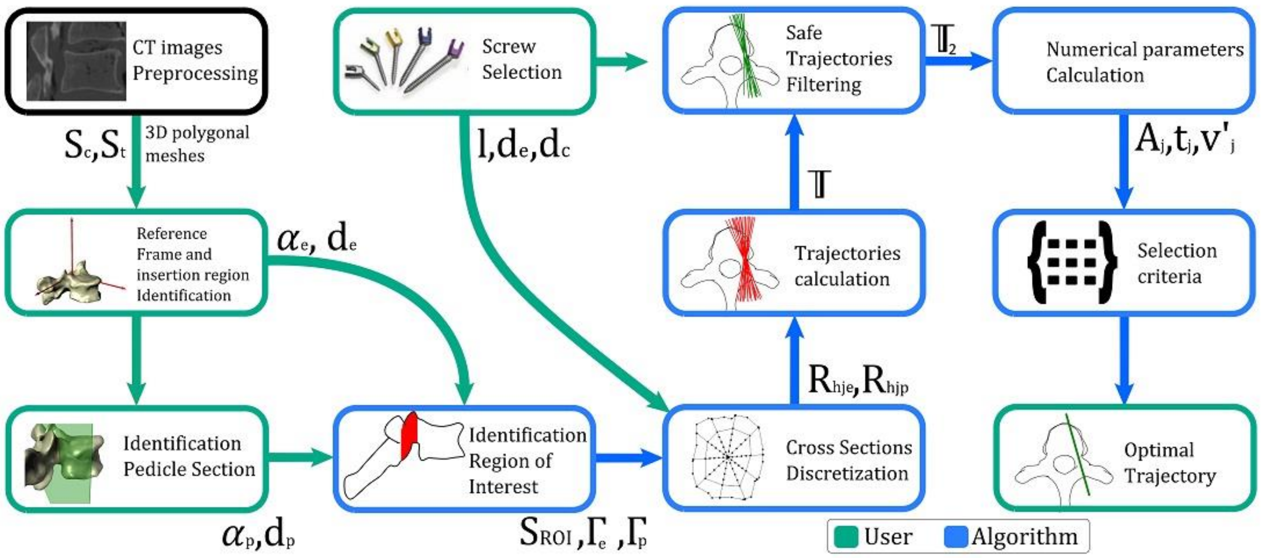


**Fig.2: Algorithm framework and interface. Green and Blue colors are used to distinguish the User inputs from the algorithm automatically executed phases to obtain the Optimal Trajectory.**

## 2.2 Reference frame and Identification of the Region of Interest

The algorithm uses 3D surface reconstructions (imported as triangulated surfaces in STL format) of both the cortical ($S_c$) and trabecular ($S_t$) bones obtained from CT scan segmentation with a threshold intensity as defined by Rathnayaka et al [17] targeted to estimate the cortical bone thickness [18]. For each vertebra a reference frame is assigned with a transverse plane ($\pi_t \equiv$x-y) as the bisector plane for the two endplates, frontal plane ($\pi_f$ //x-z) perpendicular to the transverse plane, and a plane parallel to the plane passing through the left and right upper edges of the posterior wall of the central vertebra [19]. This is illustrated further in Figure 3a where we drew a sagittal plane ($\pi_s \equiv$y-z) perpendicular to these two planes containing the center of the vertebral foramen.

A surgeon is usually asked to identify the pedicle screw dimensions such as: length (*l*), external ($d_{ext}$) and core ($d_{core}$) diameters and two planes identifying the clearance between the screw tread surface and the external bone layer. The two planes, characterizing the pedicle section and the entry region are identified by the sagittal positions $d_p$ and $d_e$ as well as the rotation angles $\alpha_p$ and $\alpha_e$ around the z-axis (see Fig.3b).

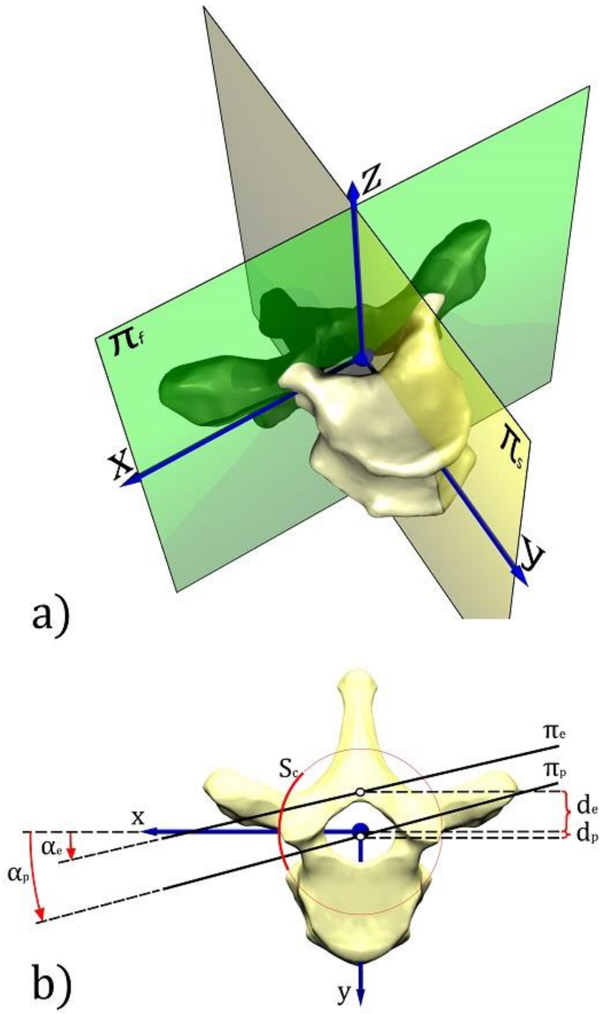


**Fig.3: a) Reference Frame adopted and b) Insertion Screw region and pedicle reference planes.**

The first section plane ($\pi_p$) should be positioned to correspond to the smallest cross section area of the pedicle whereas the second plane ($\pi_e$) should be positioned proximal to the triangular region formed by the superior articular process, the transverse process, and the pars inter-articularis [20]. The latter is largely adopted for localizing the placement of the pedicle probe [21,22]. The resulting planes are expressed as follows:

$$\pi_e \rightarrow \sin(\alpha_e)x + \cos(\alpha_e)y = \cos(\alpha_e)d_e \qquad (1)$$

$$\pi_p \rightarrow \sin(\alpha_p)x + \cos(\alpha_p)y = \cos(\alpha_p)d_p \qquad (2)$$

The Region of Interest ($S_{ROI}$) in the posterior arch is now defined as the volume of the hemi vertebra portion ($S_c \cap \pi_s^+$) limited in the anterior direction by the plane defined by the pedicle ($\pi_p$), and in the caudal direction by the plane ($\pi_{pt}$) which is parallel to the transverse plane ($\pi_t$). The latter is a plane passing through the inferior edge of the pedicle section ($P_p = min_z(\Gamma_p = (S_c \cap \pi_s^+) \cap \pi_p)$) in the transverse plane *z* direction, and is limited in the lateral direction by a cylindrical surface ($S_{cil}$) with cranial direction, surrounding the articular facets, with the aim of removing the transverse process (Fig.4a).

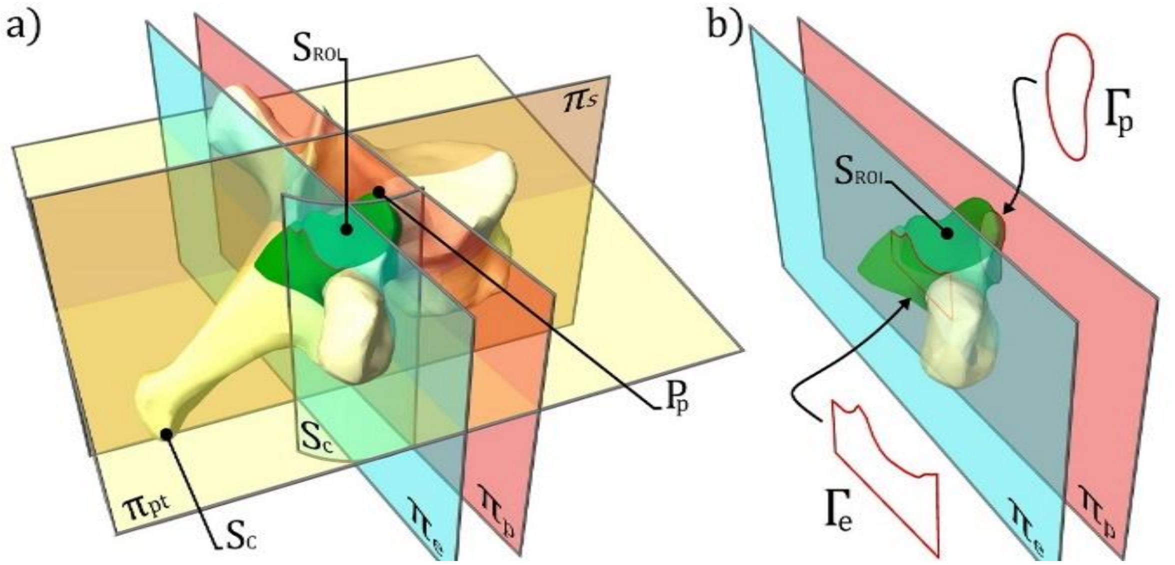


**Fig.4: a) Identification of the Region of Interest $S_{ROI}$; b) Identification of the two Cross-sections polygons $\Gamma_e$ and $\Gamma_p$ used.**

The surface $S_{cil}$, contains the highest point of the superior articular facet ($P_a = max_z(S_c \cap \pi_s^+)$) and is defined introducing a user-defined distance ($d_c$). This is given by

$$S_{cil} \rightarrow x^2 + y^2 = \left(d_c + \sqrt{(P_a \cdot \hat{x})^2 + (P_a \cdot \hat{y})^2}\right)^2 \qquad (3)$$

## 2.3 Cross Sections discretization

The trajectories are calculated by the discretization (detailed in Appendix A) of the two cross-sections $\Gamma_p$ and $\Gamma_e$ = $(S_{ROI} \cap \pi_e)$ obtained by the intersections of the computed surface $S_{ROI}$ with the two defined planes $\pi_e$ and $\pi_p$ (see Fig.4b).

The safe points ($R_{hjk}$) are identified in the k-section as a particle center mass

$$R_{hjk} = C_k \frac{\left| \left( \frac{|Q_{kj} - C_k| - d}{n_{kl}} \right) h - |Q_{kj} - C_k| \right|}{|Q_{kj} - C_k|} + Q_{kj} \left| \frac{\left( \frac{|Q_{kj} - C_k| - d}{n_{kl}} \right) h}{|Q_{kj} - C_k|} \right| \quad (4)$$

$$\text{for } j = 0,1,\ldots(n_{kb} - 1) \text{ and for } h = 0,1,\ldots(n_{kl} - 1)$$
$$|Q_{kj} - C_k| - d > 0$$

where: the point $C_k$ is the centroid of the cross- section, the points $Q_{kj}$ are a user defined number ($n_{kb}$) of equally spaced points on the k-th polygon $\Gamma_k$, $n_{kl}$ are the number of equally spaced points desired on the segments $Q_{kj}$-$C_k$ and the value of the distance $d$ is equivalent to the sum of the desired residual bone thickness $r$ and the screw external radius augmented by the maximal angular incidence β.

$$d = r + \frac{d_e}{2} \cos \beta \qquad (5)$$

This geometric structure is similar to the template proposed by Veksler for image segmentation. Has been adopted for its intrinsic attitude of distributed non-uniform nodes [23] that are closer to the cross section centroid (Fig.5), used as the reference for the screw insertion [15,24] and are here assumed as “soft spot” for the probing [10,11,21].

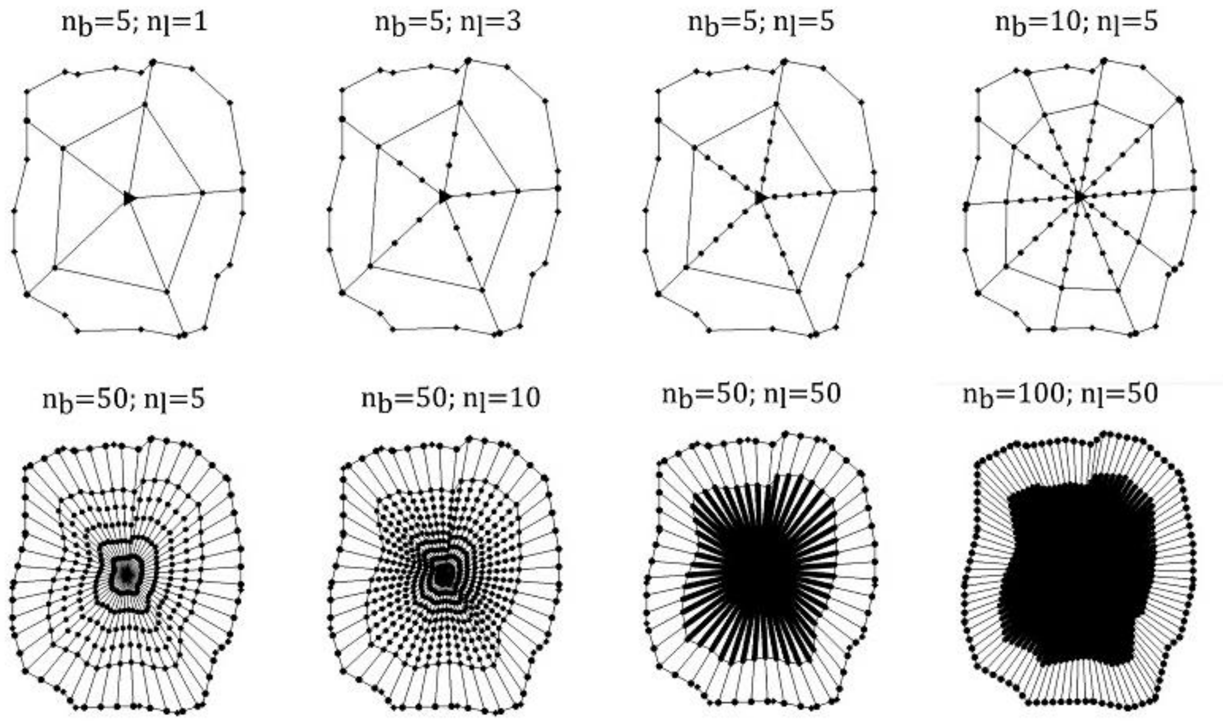


**Fig.5: Generic cross-section discretization for different configurations of the divisions imposed through the parameters $n_b$ and $n_l$.**

## 2.4 Screw Trajectories calculation

All possible $(n_{pb} \times n_{pl}) \times (n_{eb} \times n_{el})$ screw trajectories T are calculated from the $R_{hjk}$ points (Fig. 6a) and are given by the following parametric representation:

$$\begin{pmatrix} x \\ y \\ z \end{pmatrix}_{ij} = R_{hje} + t\widehat{v_{ij}} \;\; where: \widehat{v_{ij}} = \frac{(R_{hip} - R_{hje})}{|R_{hip} - R_{hje}|} \qquad (6)$$

$$for\ \mathrm{i} = 0,1, \dots \left(\mathrm{n}_{pb} - 1\right) * \left(\mathrm{n}_{pl} - 1\right) \text{ and for } \mathrm{j} = 0,1, \dots (\mathrm{n}_{eb} - 1) * (\mathrm{n}_{el} - 1)$$

## 2.5 Safe trajectories filtering

Applying two filters on the calculated trajectories T identifies the safe trajectories $T_2$. The first filter identifies the safe trajectories passing thought a referenced section of the vertebral body (see Fig.6b) and is created following these steps:

First Filter

1) The vertebral body centroid ($C_{vb}$) is evaluated as the centroid of the volume of the hemi vertebra posteriorly limited by the pedicle plane ($S_b = ((S_c \cap \pi_s^+) \cap \pi_p^+)$);
2) The intersection of the identified vertebral body volume with the frontal plane passing through the vertebral body centroid results in the cross section ($\Gamma_b = (S_b \cap \pi_{pf}) | (\pi_{pf} || \pi_f) \wedge (C_{vb} \in \pi_{pf})$).
3) The polygon ($\Gamma_b$) is divided in the same number of equally spaced points used for the pedicle ($n_b$).
4) The limits of the reference section ($S_r$) are identified at a distance ($d$) on the lines connecting the calculated points on $\Gamma_b$ with its centroid.
5) From the calculated trajectories T, are kept the trajectories $T_1$ intersecting the reference section; $((T_1 \subseteq T: \forall l_i \in T_1 \rightarrow \exists (l_i \cap S_r))$.

Second Filter

The second filter removes the trajectories with distance between the two points intercepting the vertebral surface ($S_c \cap \pi_s^+$) in the posterior arch ($E_i$) and the vertebral body ($O_i$) that are smaller than the screw length augmented by the user-defined safe dimension ($l' = l + s$)(Fig. 6b); ($T_2 \subseteq T_1: \forall l_i \in T_2 \rightarrow |E_i - O_i| < l'$).

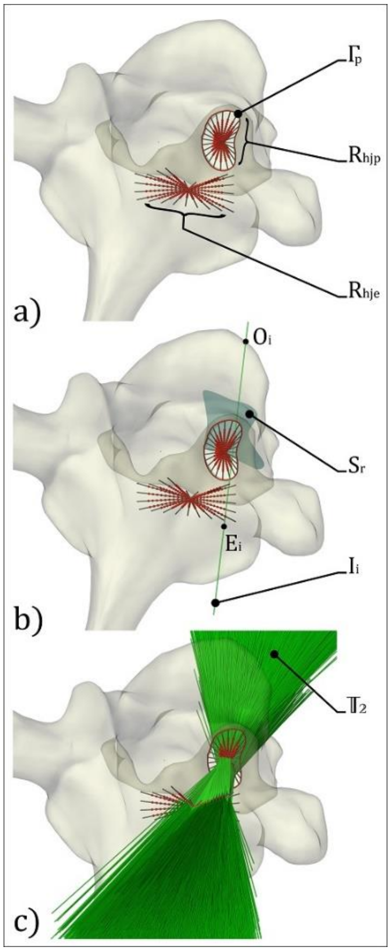


**Fig.6: Application of the method on a T3 vertebra, with $n_{pb}= n_{eb}=25$ and $n_{pl}=n_{el}=10$ are obtained: a) Cross sections discretization b) geometric representation of the filters adopted and c) Final Safe trajectories outcome.**

## 2.6 Clinically relevant insertion parameters

The safe trajectories $T_2$ (Fig. 6c) are grouped into subgroups $T_{2j}$, with their perspective entry points labeled as $E_j$. These trajectories subgroups are identified more specifically by their transverse angle $\alpha_t$ (see Fig. 7), and merged in 12 intervals of 5 degrees as follows: ($T_{2j} \subseteq T_2$: $\forall\, l_i \in T_{2j} \rightarrow ((j-1)(30/6)-30) \leq cos^{-1}((((O_i-E_i)\cdot \underline{y})\underline{y}+((O_i-E_i)\cdot \underline{x})\underline{x})/|((O_i-E_i)\cdot \underline{z})\underline{z}+((O_i-E_i)\cdot \underline{x})\underline{x}|)\cdot \underline{y}) < ((j(30/6)-30)$ *for* $j=1...12$. This stratification of subgroups is used to assure that the optimum path, its angle, and entry point selection are idealized for the patient and provide alternatives solutions to the surgeon.

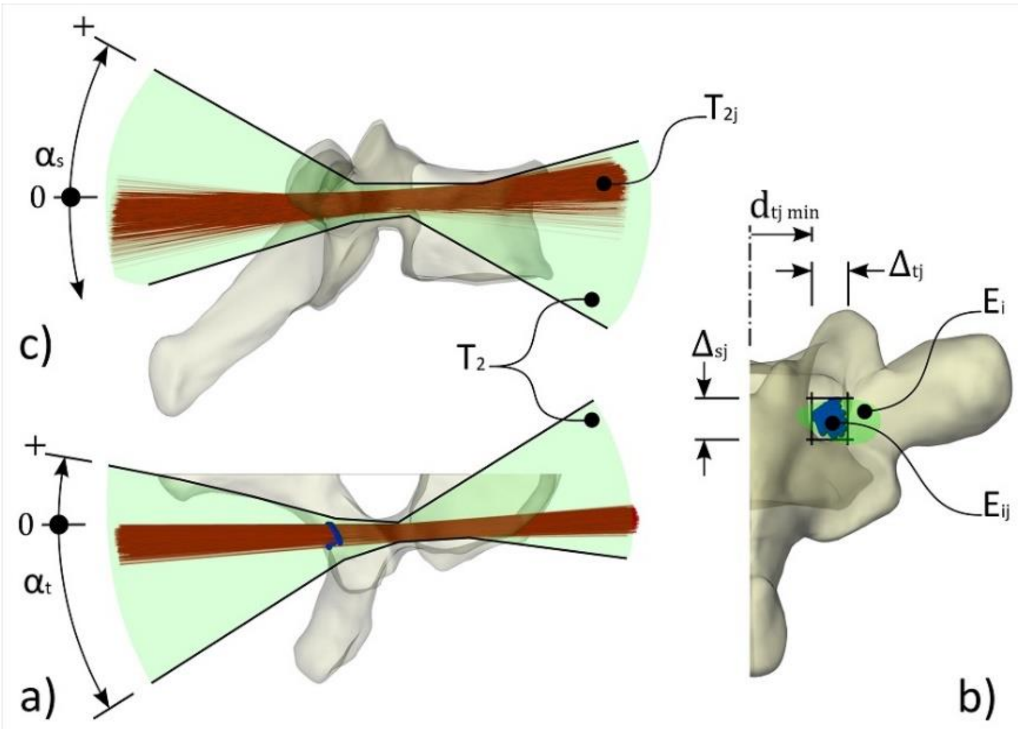


**Fig.7: Right vertebra hemi portion and corresponding safe trajectories $T_2$: a) transverse view, b) caudal coronal view and c) sagittal view.**

The critical and measurable parameters/landmarks (see Fig. 7) calculated for each j-th subgroup as reported in Appendix B, are given to the surgeon. The identifiers used in the analysis are: the minimal transverse distance of the entry points ($d_{tj\ min}$), the transverse and sagittal ranges $\Delta_{tj}$ and $\Delta_{sj}$, the sagittal angles $\alpha_s$ and its allowable range $\Lambda_{sj}$.

## 2.7 Trajectory Selection

The optimal trajectory is evaluated for each $T_{2j}$ trajectory subgroup using the following intrinsic parameters:

- $A_j$: insertion region amplitude.
- $t_j$: Insertion region shape factor, ($t_j=1/|\Delta_{tj}-\Delta_{sj}|$) calculated using transverse and sagittal ranges.
- $v'_j$: Average Percentage of the Volume in the screw thread detecting cortical bone.

The insertion region amplitude $A_j$ is calculated as the area of the convex hull [25] of the entry points $E_{i,j}$ orthogonal projections on the least-square best-fit plane [26]. This amplitude is adopted as tolerance in the identification of the insertion points. The shape factor $t_j$ is used to measure the tolerance directionality. The cortical bone thickness penetration is measured as a percentage $v'_j$ (see Appendix C) here assumed as indicative of the mechanical anchorage in light of previous studies [27,28].

The optimal trajectories are obtained using the Analytical Hierarchy Process (AHP) proposed by Saaty [29,30] for the two cases of "CASS" and "free hand" pedicle screw placement. The calculated parameters are combined with the pairwise comparisons matrices characterized by emphasis on the volume of cortical bone for the CASS (Table 1a) and on the amplitude of the insertion area for the "free hand" (Table 1b):

$$\begin{array}{ccc} A_j & t_j & v'_j \\ 1 & 1/3 & 1/7 \\ 3 & 1 & 1/5 \\ 7 & 5 & 1 \end{array} \text{(CASS)} \qquad \begin{array}{ccc} A_j & t_j & v'_j \\ 1 & 3 & 7 \\ 1/3 & 1 & 5 \\ 1/7 & 1/5 & 1 \end{array} \text{(Free Hand)} \qquad \text{(Table 1a,b)}$$

The algorithm developed has been implemented in the programming language editor integrated into Rhinoceros 3D (Robert McNeel & Associates, Seattle, WA) for its rendering capabilities and tested on thoracic vertebrae from two cadaveric spines.

The identification of entry points, angulation, and calculation of safe trajectory are analyzed further using two thoracic spine specimens (T1 to T10) using 30mm Depuy Expedium 5.5 polyaxial screws (DePuy Synthes, Warsaw, IN) with a major diameter of 4.90 mm, minor diameter of 3.66mm, and allowable angulation of ±30 °.

Also, a sensitivity analysis on different combinations of the parameters $n_b$ and $n_l$, controlling the cross-sections discretization is reported in Appendix D.

## 3 Results

The average distance between the calculated centroids of the screw insertion points and the sagittal plane is 11.5mm ±2.0mm, with a maximal value of 16.4 mm for T1 and a minimal value of 9.5mm for T6. The average transverse range for the insertion points is 6.6mm±1.7mm with a minimal value on T5 of 2.5mm and a maximal value of 8.4mm for T10. The sagittal range for the entry points has an average value of 8.16±4.9mm and its minimal value on T5 is 2.2mm (Fig. 8).

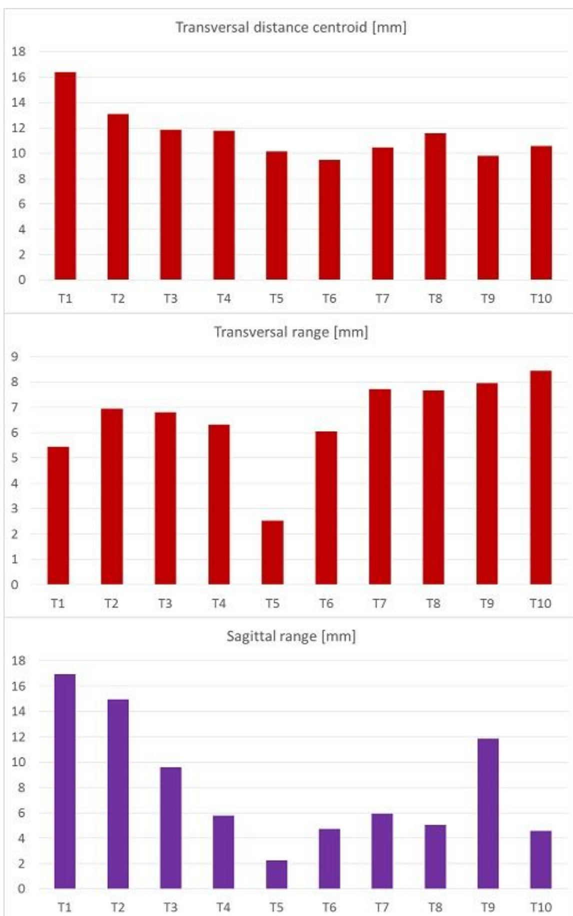

**Fig.8: Average values obtained on thoracic segments of two cadaveric spines: Transverse distances of the insertion point centroids from the sagittal plane, Transverse ranges of the insertion points $\Delta_t$ [mm] and Sagittal ranges $\Delta_s$ [mm].**

For the particular screw selected the ranges of sagittal angle $\Lambda_s$, have an average value of 41.9°±4.8°.

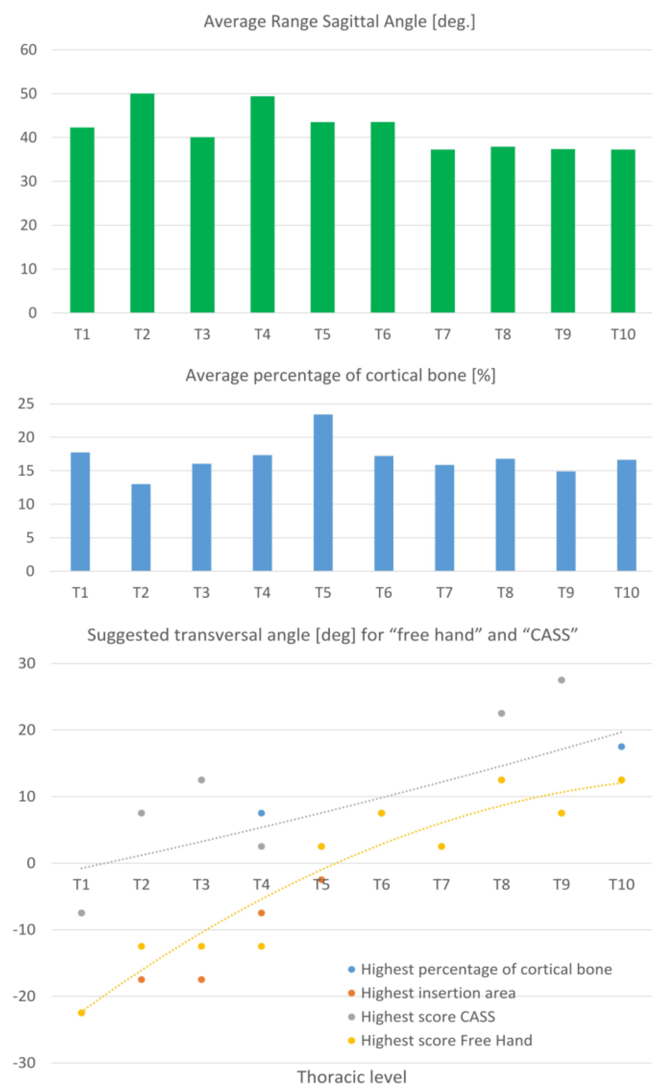


**Fig.9 Values obtained on thoracic segments of two cadaveric spines: Range of the sagittal angle ($\Lambda_s$) needed for the insertion, percentage of cortical bone detecting the screw tread *v' and* suggested transversal angles**

**according to: percentage of detected cortical bone, amplitude of the insertion area and scores obtained with AHP method for the two cases of "free hand" and "CASS" implantations.**

The range of the transverse angle is 30° in T1, 40° in T2 and T3, and reduces to 30° in T4 and T5. The angle remains constant at 5° in the lower thoracic spine (T6 to T10). The transverse angle with higher insertion area (*A*) decreased in the caudal direction from a converging angle of 22.5° at T1 to a divergent angle of 12.5° at T10 (Fig. 9b). The average percentage of cortical bone intersectiong the thread is 16.9%±2.7% and is higher at T5, with a value of 23.4% due to small pedicles characterization (Fig. 9a). The transverse angle required to maximize this percentage varied from a converging angle of 7.5° on T1 to a divergent angle of 27° at T9.

From the calculated numerical parameters, with the AHP method, in the assisted surgery, trajectories with small inclination are suggested, with 10° less in amplitude, for almost all the thoracic levels with exemption of the lower thoracic, where divergent trajectories with transverse angles up to 27.5° can intercept more cortical bone. In the case of "free hand", convergent screws are suggested from T1 to T4 and almost straight trajectories are always used for other levels, with peak values of 12.5° divergence on T10.

## 4 Discussions

The algorithm developed and highlighted in this paper requires as an initial step a 3D reconstruction of the vertebra and the position of two planes perpendicular to the transverse plane as a reference. We reconstructed the vertebra geometry using a conventional CT segmentation tool, Materialise Mimics (Materialise, Leuven, Belgium) and the segmentation did not exceed 15 minutes. This preprocessing time can be strongly reduced using techniques proposed in the literature for CT images [31–33] or by using statistical-based reconstructions requiring biplanar X-rays [34–36]. In surgical techniques involving robotic arms or templates, a planned trajectory can be replicated in surgical setting with high accuracy [7,37]. Because these techniques are based on tridimensional reconstructions of the spine [38–41], the integration with the proposed algorithm does not require additional preprocessing time. With the proposed algorithm, the surgeon defines the trajectory making use of few parameters namely two distances and two angles, whereas the current systems require all the screw's 6DOF. With "free hand" techniques the calculated optimal trajectory is communicated to the surgeon on a simulated x-ray which is limited by the preprocessing time and potential errors associated with 2D imaging. The algorithm developed in this study can improve current anatomical studies aimed to indicate proper screw placement and angulations for the "free hand" technique.

It is important to note that using a desktop workstation (Intel Xeon 3.6 GHz with 8 Gb RAM, Dell Precision, Dell Inc. Round Rock, TX) the safe trajectories calculation did not necessitate a significant amount of processing time while the calculation of the "Percentage of the Volume in the screw thread detecting cortical bone" ($v'_j$) varied according to the discretization parameters $n_b$ and $n_l$ from 2 to 20 minutes.

The developed algorithm identifies the optimal trajectory using a limited number of parameters, it does not account for parameters not geometrically quantifiable, such as bone adaptation or stress shielding, but it is the first analytical approach that provide safe screw trajectories. In previous studies, vertebral bone density has been documented to be inversely proportional to spinal implant rigidity [42] and to the changes in stresses at the bone implant interface [43–46]. A methodological approach to spine screw stress alteration has been proposed by Gefen et al. [47] that defined dimensionless parameters to measure the stress transfer between the threads and the intercepted bone. Using finite element analysis, different screw designs were evaluated and their stress shielding and consequential bone resorption was investigated [48,49]. Such parameters can be integrated with the proposed algorithm to account for the screw trajectory selection and stress shielding, using the AHP proposed method.

The developed algorithm has produced clinical relevant screw insertion parameters in agreement with previous anatomical studies. In the cranial direction, the lateral movement of the insertion point reported by Kim et al. [11] was found on both tested spines. The range of safe insertion transverse angles have a large amplitude that are seen to be directly related to the effective insertion area that is not uniformly distributed in the lower thoracic spine. The transverse angles associated with the trajectories with highest insertion area are in agreement with the transverse pedicle angles found by Zindrick et al. [13]. In previously developed anatomical studies, the pedicle dimension was used as an indicator of the amplitude of the insertion region [13,14,50–52], while the proposed algorithm indicates on the posterior cortex the actual amplitude of the safe insertion region and the required insertion angles. A limitation is the calculation of the percentage of screw thread volume in contact with the cortical bone ($v_j$). Another limitation is the number of specimen and spines used to validate our algorithm; this will be increased in future studies. The proposed method, being pedicle arch based, applies to vertebrae characterized by strong morphological alterations such as posterior element disruption and facet joint hypertrophy [16]. The screw insertion errors related to the variability between the left and right sides of the distance between the posterior and anterior cortex (here indicated as $|E_i-O_i|$) reported by Cui et al. [52] are excluded by the filter conditions adopted.

## Conclusion

The proposed algorithm works well with CT data commonly available for most patients undergoing spinal fusion or correction. The method allows proper screw selection for safe trajectories and calculates critical values such as screw inclinations and volume of cortical bone intersected. To our knowledge, the proposed method is the first that uses an analytical approach for the screw placement.

## Ethical approval

Not required.

## Acknowledgements

The work has been developed in the Biomechanics Research Laboratory of the Department of Orthopaedics, University of Illinois at Chicago and was partially supported by the Aurelio M. Caccomo Family Foundation. The authors would also like to thank Mr. Cory Helder for proof reading the manuscript.

## Conflict of interest statement

Nothing to declare.

## Appendix A: Cross Sections discretization

Consider two polygons as shown in Figure 4 that pass through a set of data points determined by registration or identified and selected by some imaging techniques such as CT or a trained surgeon. The two polygons $\Gamma_p$ and $\Gamma_e = (S_{ROI} \cap \pi_e)$ are made of a set data points referred to as $np_e$ utilizing points $P_{ei}$ points. Similarly, we have $np_p$ points utilizing $P_{pi}$. Both of these polygons have total lengths of $\lambda_p$ and $\lambda_e$ respectively where,

$$\lambda_k = \left|P_{k(np_k)} - P_{k0}\right| + \sum_0^{(np_k-1)} \left|P_{k(i+1)} - P_{ki}\right| \quad where\ k = \begin{cases} p \\ e \end{cases} \qquad \text{(A.1)}$$

To generate a number of screw trajectories independently from the Polygonal mesh adopted, a user defined number of equally spaced points $Q_{kj}$ are created on the k-th polygon $\Gamma_k$ (Fig.A.1). Furthermore, we impose the condition that the first point $Q_{k0}$ coincides with point $P_{k0}$ and used as a reference ($Q_{K0}$=$P_{K0}$).

The m-th segment ($P_{k(m+1)}$-$P_{km}$) containing the $j$-th point $Q_{kj}$ is simply defined by the distance $j(\lambda_k/n_{kb})$ denoted by

$$m \in \mathbb{N}^+ : \lambda_{(m+1)k} > \frac{\lambda_k}{n_{kb}}(j) \geq \lambda_{mk} \quad for\ j = 0,..(n_{kb}-1) \qquad \text{(A.2)}$$

We further compute all the relative lengths $\lambda_{mk}$ for all $P_{ki}$ points as distance from the initial reference point $P_{k0}$ as follows;

$\lambda_{mk} = \sum_{i=1}^{m} \left| P_{k(i)} - P_{k(i-1)} \right| \; with \; \lambda_{0k} = 0 \;\; and \; \lambda_{(np_{k+1})k} = \lambda_k$ (A.3)

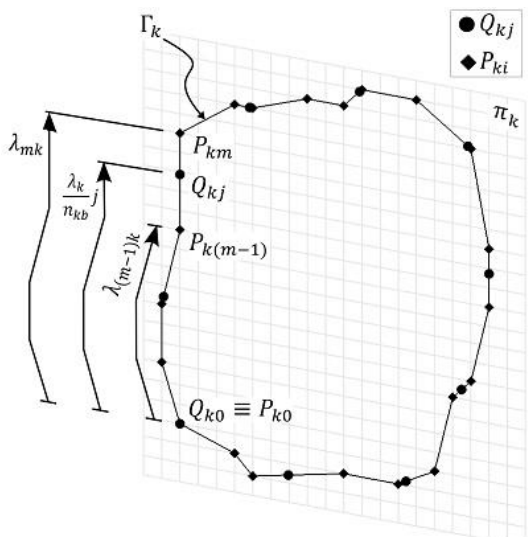


**Fig. A.1: Generation of the equally spaced points $Q_{kj}$ on a generic planar polygon $\Gamma_k$ composed by the points $P_{ki}$.**

Once the *m*-th segment has been computed, the equally spaced points are than calculated as the distance to the center of mass of the segment where the relative weights are reduced by the distance of prior computed point $Q_{k(j-1)}$ from the $P_{k(m-1)}$.

$$Q_{kj} = P_{k(m-1)} \left( 1 - \frac{\left( \left( {}^{\lambda_k}/_{n_{kb}} \right) * j - \lambda_{(m-1)k} \right)}{\lambda_{mk} - \lambda_{(m-1)k}} \right) + P_{km} \frac{\left( \left( {}^{\lambda_k}/_{n_{kb}} \right) * j - \lambda_{(m-1)k} \right)}{\lambda_{mk} - \lambda_{(m-1)k}} \quad \text{(A.4)}$$

The equally spaced points ($Q_{kj}$) identified on the section profile are connected to the centroid ($C_k$) used as a seed point to generate the safe region.

The centroid $C_k$ of the k-th section is calculated by geometric decomposition where the unit figures are the triangles formed by each *s*-th polygon's segment intersecting plane $\pi_k$ (see Fig.A.2).

$$C_k = \frac{\sum_{s=0}^{np_k - 1} A_{ks} \, C_{ks}}{\sum_{s=0}^{np_k - 1} A_{ks}} \qquad \text{(A.5)}$$

For the *s*-th segment, we define its center $C_{ks}$ making use of the vertices where

$$C_{ks} = \frac{P_{k(i+1)}+P_{ki}+d_k\hat{y}}{3} \;\; where: P_{k(np_k+1)} = P_{k0} \qquad \text{(A.6)}$$

It follows that its cross section area $A_{ks}$ is found by using the cross product of the position vector's projections $P'_{ki}$ and can be defined as

$$A_{ks} = \frac{1}{2}\left(P'_{ik} \times P'_{(i+1)k}\right) \cdot \begin{pmatrix} \sin\alpha_k \\ \cos\alpha_k \\ 0 \end{pmatrix} \; where: P'_{ik} = P_{ik} - d_k\hat{y} \qquad \text{(A.7)}$$

Starting at the distance (*d*) from $Q_{kj}$ and subdividing the remaining portion of the connecting lines in equally spaced segments $n_{kl}$ we create the *k* points for the segments $Q_{kj}$-$C_k$ which is longer than *d* (Fig. A.2).

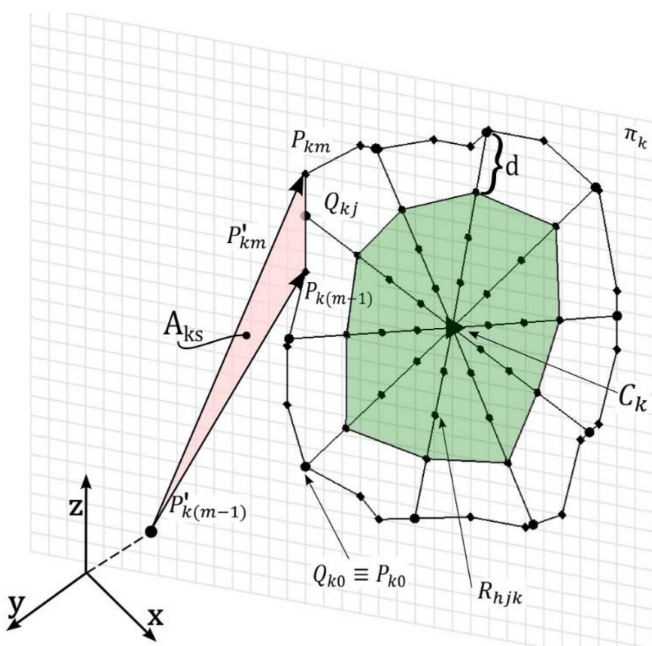


**Fig. A.2: Geometric representation of the cross-section discretization adopted.**

Using the hypothesis that a "star shape" characterizes both cross sections, the safe points ($R_{hjk}$) are identified in the k-section as a particle center mass

$$R_{hjk}=C_k\frac{\left|\left(\frac{|Q_{kj}-C_k|-d}{n_{kl}}\right)h-|Q_{kj}-C_k|\right|}{|Q_{kj}-C_k|}+Q_{kj}\left|\frac{\left(\frac{|Q_{kj}-C_k|-d}{n_{kl}}\right)h}{|Q_{kj}-C_k|}\right| \quad \text{(A.8)}$$
$$\text{for } j=0,1,\ldots(nkb-1) \text{ and for } h=0,1,\ldots(nkl-1)$$
$$|Q_{kj}-C_k|-d>0$$

where the centroid of the cross- section ($C_k$), the value of the distance *d* is equivalent to the sum of the desired residual bone thickness *r* and of the screw external radius augmented by the maximal angular incidence β.

$$d = r + \frac{d_e}{2}\cos\beta \qquad \text{(A.9)}$$

**Appendix B: Insertion parameters calculation**

The minimal transverse distance of the entry points ($d_{tj\ min}$) is calculated by evaluating the position of the closest point to the sagittal plane

$$d_{tj\ min} = |E_{t\ min}\cdot\hat{x}|\ |\forall E_i \in T_{2j}\ \ |E_{t\ min}\cdot\hat{x}|\ \le |E_i\cdot\hat{x}| \quad \text{(B.1)}$$

The transverse range $\Delta_{tj}$=$d_{tj\ max}$-$d_{tj\ min}$ is defined by the transverse distance between the closest and furthest point in the transverse direction

$$d_{tj\ max} = |E_{t\ max}\cdot\hat{x}|\ |\forall E_i \in T_{2j}\ \ |E_{t\ max}\cdot\hat{x}|\ \ge |E_i\cdot\hat{x}| \quad \text{(B.2)}$$

The sagittal range $\Delta_{tj}$=$d_{sj\ max}$-$d_{sj\ min}$ is similarly defined by the positions of the highest

$$d_{sj\ max} = |E_{s\ max}\cdot\hat{z}|\ |\forall E_i \in T_{2j}\ \ |E_{s\ max}\cdot\hat{z}|\ \ge |E_i\cdot\hat{z}| \quad \text{(B.3)}$$

and of the lowest entry points

$$d_{sj\ min} = |E_{s\ min}\cdot\hat{z}|\ |\forall E_i \in T_{2j}\ \ |E_{s\ min}\cdot\hat{z}|\ \le |E_i\cdot\hat{z}| \quad \text{(B.4)}$$

The average value of the angles in the sagittal plane, sagittal angles $\alpha_s$, and its range ($\Lambda_{sj}$) are defined as follows;

$$\alpha_{s\ j} = \cos^{-1}\left(\frac{\left(((O_i-E_i)\cdot\hat{y})\hat{y}+((O_i-E_i)\cdot\hat{z})\hat{z}\right)}{|((O_i-E_i)\cdot\hat{y})\hat{y}+((O_i-E_i)\cdot\hat{z})\hat{z}|}\cdot\hat{y}\right)\quad \forall\ E_J \in T_{2j} \qquad \text{(B.5)}$$

$\Lambda_{sj} = \max(\alpha_{s\,i}) - \min(\alpha_{s\,i})$ (B.6)

## Appendix C: Percentage of the Volume in the screw thread detecting cortical bone (*v'j*)

For each safe trajectory $l_i$, with norm $ni_i = (O_i - E_i)/|O_i - E_i|$, we identified the volumes intercepted on cortical $Vcort_i$ and trabecular bone volumes $Vtrab_i$ between the cylinder $S_{ext,i}$ which as a diameter equivalent to the screw external diameter and the cylinder $S_{core,i}$ with a screw core diameter limited on the entry points and screw length l by planes $\pi_{ins\,i}$ and $\pi_{end\,i}$.

$$S_{ext,i} \rightarrow {K_0}^2 + {K_1}^2 = \left(\frac{d_{ext}}{2}\right)^2 \quad \text{(C.1)}$$

$$S_{core,i} \rightarrow {K_0}^2 + {K_1}^2 = \left(\frac{d_{core}}{2}\right)^2 \quad \text{(C.2)}$$

where:

$$K_0 = -x\sin\theta + y\cos\theta\cos\varphi + z\cos\theta\sin\varphi \quad \text{(C.3)}$$

$$K_1 = -y\sin\varphi + z\cos\varphi \quad \text{(C.4)}$$

with:

$$\theta = \tan^{-1}\left(\frac{ni_i \cdot \hat{y}}{ni_i \cdot \hat{x}}\right)\ and\ \varphi = \sin^{-1}(ni_i \cdot \hat{z}) \quad \text{(C.5)}$$

and the limiting planes are:

$$\pi_{ins,i} \rightarrow ni_i \cdot \hat{x}(x - E_i \cdot \hat{x}) + ni_i \cdot \hat{y}(y - E_i \cdot \hat{y}) + ni_i \cdot \hat{z}(z - E_i \cdot \hat{z}) = 0 \quad \text{(C.6)}$$

$$\pi_{end,i} \rightarrow ni_i \cdot \hat{x}(x - (E_i + ni_i l) \cdot \hat{x}) + ni_i \cdot \hat{y}(y - (E_i + ni_i l) \cdot \hat{y}) + ni_i \cdot \hat{z}(z - (E_i + ni_i l) \cdot \hat{z}) = 0 \quad \text{(C.7)}$$

The $v'_j$, is calculated as the average of the values $v_{i,j} = 100*(Vcort_i - Vtrab_i)/(Vcort_i)$ where the volumes are:

$$Vcort_i = S_c \cap \left(\left(\left(S_{ext,i} - S_{core,i}\right) \cap {\pi_{ins,i}}^{+}\right) \cap {\pi_{ins,i}}^{-}\right) \quad \text{(C.8) and}$$

$$Vtrab_i = S_t \cap \left(\left(\left(S_{ext,i} - S_{core,i}\right) \cap {\pi_{ins,i}}^{+}\right) \cap {\pi_{ins,i}}^{-}\right) \text{(C.9)}$$

## Appendix D: Sensitivity Analysis of parameters $n_b$ and $n_l$, controlling the cross-sections discretization.

Based on a randomly selected set of vertebra from the thoracic segments obtained from two subjects the entry points are computed for different combinations of $n_b$ and $n_l$, controlling the cross-sections discretization. Both polygons $\Gamma_p$ and $\Gamma_e$ are also discretized with the same numbers of points ($n_b=n_{pb}=n_{eb}$) ranging from 15 to 30. Similarly, lines connecting the edges with the centroids are discretized with three values ranging from 10 to 20. The safe trajectories are found within the range of the transverse angles ranging from 10° (divergent screws) to values greater than -30° (convergent screws). The highest range for the sagittal angle is found when the transverse angle is between 20° and 25°.

For the most divergent trajectories in the range of 5° to 10°, we found no statistical differences in the sagittal angle (F=0.041), the insertion cross-section area (F=0.170) and the transversal position of the centroid (F=0.295). When also analyzed how $n_l$, and $n_b$ influence the transversal trajectories. Hence, the optimum safe trajectories can be found by dividing further the lines ($n_l=10$), to reduce the computational cost, and the number of points representing the different cross sections ($n_b=30$).

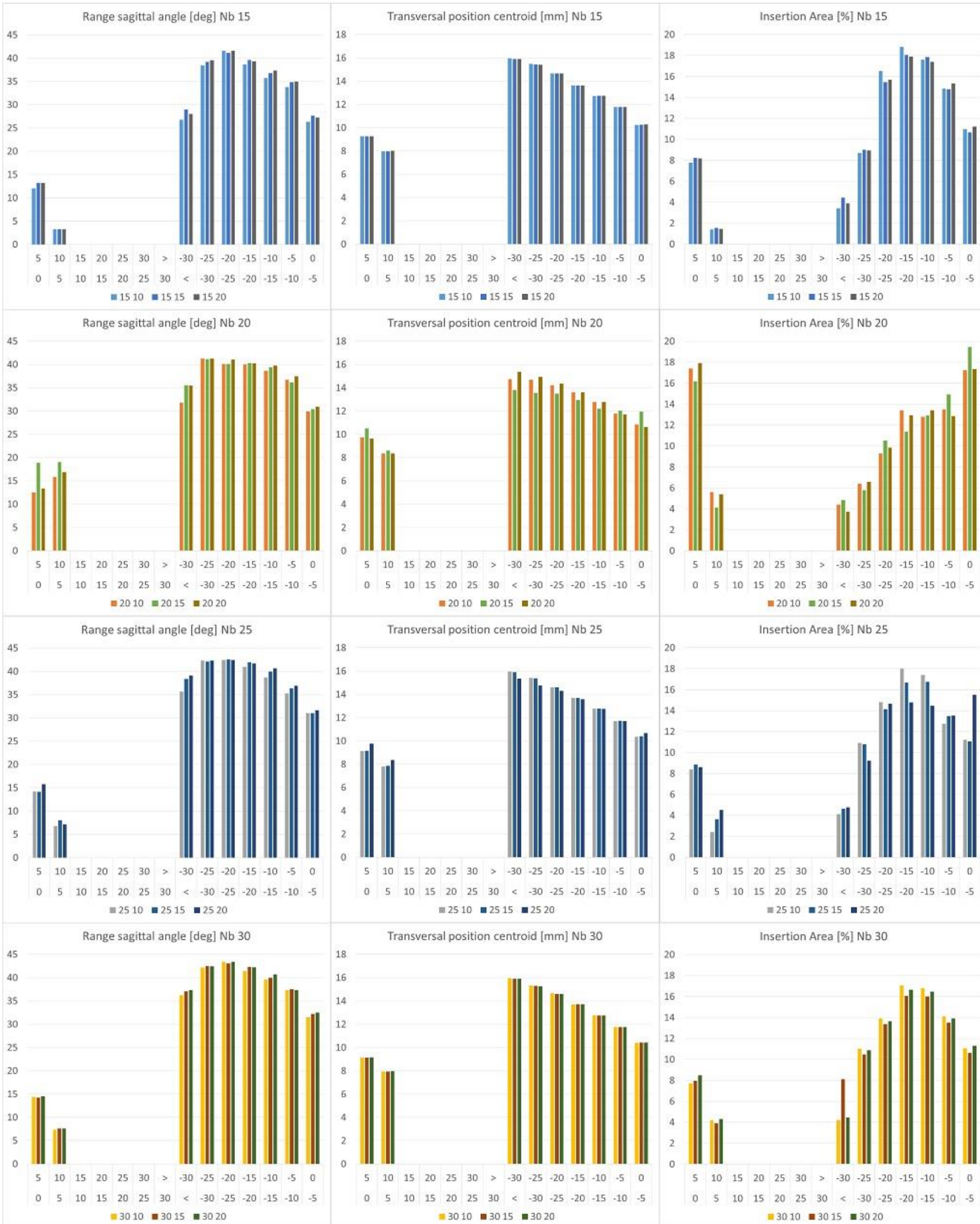


**Fig. D.1: Results obtained for each Transverse angle subgroup for a random thoracic vertebra for combinations of values $n_b$ and $n_l$ values controlling the cross-sections discretization: the safe trajectories range from 10° of divergence to 30 of convergence (shown as a negative number).**

**References:**


[1] Dobbs MB, Lenke LG, Kim YJ, Kamath G, Peelle MW, Bridwell KH. Selective posterior thoracic fusions for adolescent idiopathic scoliosis: comparison of hooks versus pedicle screws. Spine (Phila Pa 1976) 2006;31:2400–4.

[2] Di Silvestre M, Parisini P, Lolli F, Bakaloudis G. Complications of thoracic pedicle screws in scoliosis treatment. Spine (Phila Pa 1976) 2007;32:1655–61.

[3] Hicks JM, Singla A, Shen FH, Arlet V. Complications of pedicle screw fixation in scoliosis surgery: a systematic review. Spine (Phila Pa 1976) 2010;35:465–70.

[4] Privitera DM, Matsumoto H, Gomez JA, Roye DP, Hyman JE, Vitale MG. Are Breech Rates for Pedicle Screws Higher in the Upper Thoracic Spine? Spine Deform 2013;1:189–95.

[5] Cardoso MJ, Helgeson MD, Paik H, Dmitriev AE, Lehman RA, Rosner MK. Structures at risk from pedicle screws in the proximal thoracic spine: computed tomography evaluation. Spine J 2010;10:905–9.

[6] Verma R, Krishan S, Haendlmayer K, Mohsen A. Functional outcome of computer-assisted spinal pedicle screw placement: a systematic review and meta-analysis of 23 studies including 5,992 pedicle screws. Eur Spine J 2010;19:370–5.

[7] Lu S, Zhang YZ, Wang Z, Shi JH, Chen YB, Xu XM, et al. Accuracy and efficacy of thoracic pedicle screws in scoliosis with patient-specific drill template. Med Biol Eng Comput 2012;50:751–8.

[8] Abe Y, Ito M, Abumi K, Kotani Y, Sudo H, Minami A. A novel cost-effective computer-assisted imaging technology for accurate placement of thoracic pedicle screws. J Neurosurg Spine 2011;15:479–85.

[9] Lehman R a, Polly DW, Kuklo TR, Cunningham B, Kirk KL, Belmont PJ. Straight-forward versus anatomic trajectory technique of thoracic pedicle screw fixation: a biomechanical analysis. Spine (Phila Pa 1976) 2003;28:2058–65.

[10] Lehman R a, Kuklo TR. Use of the anatomic trajectory for thoracic pedicle screw salvage after failure/violation using the straight-forward technique: a biomechanical analysis. Spine (Phila Pa 1976) 2003;28:2072–7.

[11] Kim YJ, Lenke LG. Thoracic pedicle screw placement: free-hand technique. Neurol India 2005;53:512–9.

[12] Elliott MJM, Slakey CDRJB. Thoracic pedicle screw placement: analysis using anatomical landmarks without image guidance. J Pediatr Orthop 2007;27:582–6.

[13] Zindrick MR, Wiltse LL, Doornik A, Widell EH, Knight GW, Patwardhan AG, et al. Analysis of the morphometric characteristics of the thoracic and lumbar pedicles. Spine (Phila Pa 1976) 1987;12:160–6.

[14] Lien S-B, Liou N-H, Wu S-S. Analysis of anatomic morphometry of the pedicles and the safe zone for through-pedicle procedures in the thoracic and lumbar spine. Eur Spine J 2007;16:1215–22.

[15] Rampersaud YR, Simon D a, Foley KT. Accuracy requirements for image-guided spinal pedicle screw placement. Spine (Phila Pa 1976) 2001;26:352–9.

[16] Khan SN, Patel RJ, Klineberg E, Gupta MC. The “canoe” technique to insert lumbar pedicle screws: consistent, safe, and simple. Am J Orthop (Belle Mead NJ) 2013;42:234–6.

[17] Rathnayaka K, Sahama T, Schuetz MA, Schmutz B. Effects of CT image segmentation methods on the accuracy of long bone 3D reconstructions. Med Eng Phys 2011;33:226–33.

[18] Treece GM, Gee AH, Mayhew PM, Poole KES. High resolution cortical bone thickness measurement from clinical CT data. Med Image Anal 2010;14:276–90.

[19] Danesi V, Zani L, Scheele A, Berra F, Cristofolini L. Reproducible reference frame for in vitro testing of the

human vertebrae. J Biomech 2014;47:313–8.

[20] Parker SL, McGirt MJ, Farber SH, Amin AG, Rick A-M, Suk I, et al. Accuracy of free-hand pedicle screws in the thoracic and lumbar spine: analysis of 6816 consecutive screws. Neurosurgery 2011;68:170–8; discussion 178.

[21] Boachie-Adjei O, Girardi FP, Bansal M, Rawlins B a. Safety and efficacy of pedicle screw placement for adult spinal deformity with a pedicle-probing conventional anatomic technique. J Spinal Disord 2000;13:496–500.

[22] Puvanesarajah V, Liauw J a, Lo S-F, Lina I a, Witham TF. Techniques and accuracy of thoracolumbar pedicle screw placement. World J Orthop 2014;5:112–23.

[23] Egger J, Lüddemann T, Schwarzenberg R, Freisleben B, Nimsky C. Interactive-cut: Real-time feedback segmentation for translational research. Comput Med Imaging Graph 2014;38:285–95.

[24] Sugawara T, Higashiyama N, Kaneyama S, Takabatake M, Watanabe N, Uchida F, et al. Multistep pedicle screw insertion procedure with patient-specific lamina fit-and-lock templates for the thoracic spine: clinical article. J Neurosurg Spine 2013;19:185–90.

[25] Chan TM. Optimal output-sensitive convex hull algorithms in two and three dimensions. Discrete Comput Geom 1996;16:361–8.

[26] Muralikrishnan B, Raja J. Computational surface and roundness metrology. London: Springer London; 2009.

[27] Bianco R-J, Arnoux P-J, Wagnac E, Mac-Thiong J-M, Aubin C-É. Minimizing Pedicle Screw Pullout Risks: A Detailed Biomechanical Analysis of Screw Design and Placement. J Spinal Disord Tech 2014;4.

[28] Santoni BG, Hynes RA, McGilvray KC, Rodriguez-Canessa G, Lyons AS, Henson MAW, et al. Cortical bone trajectory for lumbar pedicle screws. Spine J 2009;9:366–73.

[29] Saaty TL. Decision-making with the AHP: Why is the principal eigenvector necessary. Eur J Oper Res 2003;145:85–91.

[30] Saaty TL. Decision making with the analytic hierarchy process. Int J Serv Sci 2008;1:83.

[31] Huang J, Jian F, Wu H, Li H. An improved level set method for vertebra CT image segmentation. Biomed Eng Online 2013;12:48.

[32] Ma J, Lu L. Hierarchical segmentation and identification of thoracic vertebra using learning-based edge detection and coarse-to-fine deformable model. Comput Vis Image Underst 2013;117:1072–83.

[33] Yao J, Glocker B, Klinder T, Li S, editors. Recent advances in computational methods and clinical applications for spine imaging. Springer International Publishing AG Switzerland; 2015.

[34] Pomero V, Mitton D, Laporte S, de Guise JA, Skalli W. Fast accurate stereoradiographic 3D-reconstruction of the spine using a combined geometric and statistic model. Clin Biomech (Bristol, Avon) 2004;19:240–7.

[35] Moura DC, Boisvert J, Barbosa JG, Labelle H, Tavares JMRS. Fast 3D reconstruction of the spine from biplanar radiographs using a deformable articulated model. Med Eng Phys 2011;33:924–33.

[36] Carreau JH, Bastrom T, Petcharaporn M, Schulte C, Marks M, Illés T, et al. Computer-generated, three-dimensional spine model from biplanar radiographs: A validity study in idiopathic scoliosis curves greater than 50 degrees. Spine Deform 2014;2:81–8.

[37] Lieberman IH, Hardenbrook M a., Wang JC, Guyer RD. Assessment of Pedicle Screw Placement Accuracy, Procedure Time, and Radiation Exposure Using a Miniature Robotic Guidance System. J Spinal Disord Tech 2012;25:241–8.

[38] Lieberman IH, Togawa D, Kayanja MM, Reinhardt MK, Friedlander A, Knoller N, et al. Bone-mounted miniature robotic guidance for pedicle screw and translaminar facet screw placement: Part I - Technical

development and a test case result. Neurosurgery 2006;59:641–50.

[39] Birnbaum K, Schkommodau E, Decker N, Prescher a, Klapper U, Radermacher K. Computer-assisted orthopedic surgery with individual templates and comparison to conventional operation method. Spine (Phila Pa 1976) 2001;26:365–70.

[40] Ma T, Xu Y-Q, Cheng Y-B, Jiang M-Y, Xu X-M, Xie L, et al. A novel computer-assisted drill guide template for thoracic pedicle screw placement: a cadaveric study. Arch Orthop Trauma Surg 2012;132:65–72.

[41] Merc M, Drstvensek I, Vogrin M, Brajlih T, Recnik G. A multi-level rapid prototyping drill guide template reduces the perforation risk of pedicle screw placement in the lumbar and sacral spine. Arch Orthop Trauma Surg 2013;133:893–9.

[42] McAfee PC, Farey ID, Sutterlin CE, Gurr KR, Warden KE, Cunningham BW. The effect of spinal implant rigidity on vertebral bone-density - a canine model. Spine (Phila Pa 1976) 1991;16:S190–7.

[43] Lim T-H, Goel VK, Weinstein JN, Kong W. Stress analysis of a canine spinal motion segment using the finite element technique. J Biomech 1994;27:1259–69.

[44] Hussain M, Natarajan RN, Fayyazi AH, Braaksma BR, Andersson GBJ, An HS. Screw angulation affects bone-screw stresses and bone graft load sharing in anterior cervical corpectomy fusion with a rigid screw-plate construct: a finite element model study. Spine J 2009;9:1016–23.

[45] Ahn Y-H, Chen W-M, Lee K-Y, Park K-W, Lee S-J. Comparison of the load-sharing characteristics between pedicle-based dynamic and rigid rod devices. Biomed Mater 2008;3:044101.

[46] Tsubota KI, Adachi T, Tomita Y. Effects of a fixation screw on trabecular structural changes in a vertebral body predicted by remodeling simulation. Ann Biomed Eng 2003;31:733–40.

[47] Gefen A. Optimizing the biomechanical compatibility of orthopedic screws for bone fracture fixation. Med Eng Phys 2002;24:337–47.

[48] Gefen A. Computational simulations of stress shielding and bone resorption around existing and computer-designed orthopaedic screws. Med Biol Eng Comput 2002;40:311–22.

[49] Be'ery-Lipperman M, Gefen A. A method of quantification of stress shielding in the proximal femur using hierarchical computational modeling. Comput Methods Biomech Biomed Engin 2006;9:35–44.

[50] Weinstein JN, Rydevik BL, Rauschning W. Anatomic and technical considerations of pedicle screw fixation. Clin Orthop Relat Res 1992:34–46.

[51] Abuzayed B, Tutunculer B, Kucukyuruk B, Tuzgen S. Anatomic basis of anterior and posterior instrumentation of the spine: morphometric study. Surg Radiol Anat 2010;32:75–85.

[52] Cui G, Watanabe K, Hosogane N, Tsuji T, Ishii K, Nakamura M, et al. Morphologic evaluation of the thoracic vertebrae for safe free-hand pedicle screw placement in adolescent idiopathic scoliosis: a CT-based anatomical study. Surg Radiol Anat 2012;34:209–16.

**Figures:**

Fig.1 2d Visualization of Screw placements on axial CT image of T1.

Fig.2: Algorithm framework and interface. Green and Blue colors are used to distinguish the User inputs from the algorithm automatically executed phases to obtain the Optimal Trajectory.

Fig.3: a) Reference Frame adopted and b) Insertion Screw region and pedicle reference planes.

Fig.4: a) Identification of the Region of Interest $S_{ROI}$; b) Identification of the two Cross-sections polygons $\Gamma_e$ and $\Gamma_p$ used.

Fig.5: Generic cross-section discretization for different configurations of the divisions imposed through the parameter $n_b$ and $n_l$.

Fig.6: Application of the method on a T3 vertebra, with $n_{pb}= n_{eb}=25$ and $n_{pl}=n_{el}=10$ are obtained: a) Cross sections discretization b) geometric representation of the filters adopted and c) Final Safe trajectories outcome.

Fig.7: Right vertebra hemi portion and corresponding safe trajectories $T_2$: a) transverse view, b) caudal coronal view and c) sagittal view.

Fig.8: Average values obtained on thoracic segments of two cadaveric spines: Transversal distances of the insertion point centroids from the sagittal plane, Transversal ranges of the insertion points $\Delta_t$ [mm] and Sagittal ranges $\Delta_s$ [mm].

Fig.9: Values obtained on thoracic segments of two cadaveric spines: Range of the sagittal angle ($\Lambda_s$) needed for the insertion, percentage of cortical bone detecting the screw tread *v' and* suggested transversal angles according to: percentage of detected cortical bone, amplitude of the insertion area and scores obtained with AHP method for the two cases of “free hand” and “CASS” implantations.

Fig. A.1: Generation of the equally spaced points $Q_{kj}$ on a generic planar polygon $\Gamma_k$ composed by the points $P_{ki}$.

Fig. A.2: Geometric representation of the cross-section discretization adopted.

Fig.D.1: Results obtained for each Transverse angle subgroup for a random thoracic vertebra for combinations of $n_b$ and $n_l$ values controlling the cross-sections discretization: the safe trajectories range from 10° of divergence to 30° of convergence (shown as a negative number).